NASA TECHNICAL NOTE

NASA TN D-5346

c. 1

NASA TN D-5346

TECH LIBRARY KAFB, NM
0132316

LOAN COPY: RETURN TO
AFWL (WLIL-2)
KIRTLAND AFB, N MEX

UPWASH PATTERNS ON ABLATING AND NONABLATING CONES AT HYPERSONIC SPEEDS

by John B. McDevitt and Jack A. Mellenthin

Ames Research Center
Moffett Field, Calif.

NATIONAL AERONAUTICS AND SPACE ADMINISTRATION • WASHINGTON, D. C. • JULY 1969

TECH LIBRARY KAFB, NM

0132316

1. Report No.	2. Government Accession No.	3. Recipient's Catalog No.
NASA TN D-5346		

4. Title and Subtitle
UPWASH PATTERNS ON ABLATING AND NONABLATING CONES AT HYPERSONIC SPEEDS

5. Report Date
July 1969

6. Performing Organization Code

7. Author(s)
John B. McDevitt and Jack A. Mellenthin

8. Performing Organization Report No.
A-3279

9. Performing Organization Name and Address
NASA Ames Research Center
Moffett Field, Calif. 94035

10. Work Unit No.
124-07-02-14-00-21

11. Contract or Grant No.

13. Type of Report and Period Covered
Technical Note

12. Sponsoring Agency Name and Address
National Aeronautics and Space Administration
Washington D.C. 20546

14. Sponsoring Agency Code

15. Supplementary Notes

16. Abstract

A study has been made of the upwash patterns on slender ablating and nonablating cones at angle of attack in the hypersonic flow regime. An oil-film technique was used to display the surface streamlines on the nonablating models and tests were conducted with both laminar and transitional boundary layers. The boundary-layer-edge Mach number and model wall temperature were found to have a strong influence on the magnitude of surface upwash angles. The measured surface upwash angles at small angles of attack agreed well with theoretical estimates in the laminar case. At transitional Reynolds numbers clear evidence was obtained that streamwise vortices are entrained within the boundary layer for cones at angle of attack. Tests of ablating cones at transitional Reynolds numbers resulted in upwash groove patterns eroded in the model surfaces. These grooves were interpreted to be the result of vortices intensifying local heating rates. The upward inclination of the grooves agreed closely with the inclination of the vortex paths measured on the nonablating cones under similar test conditions.

17. Key Words (Suggested by Author)	18. Distribution Statement
Cones Hypersonic viscous flow Surface streamlines Upwash Boundary-layer vortices	Unclassified - Unlimited

19. Security Classif. (of this report)	20. Security Classif. (of this page)	21. No. of Pages	22. Price
Unclassified	Unclassified	32	$3.00

UPWASH PATTERNS ON ABLATING AND NONABLATING CONES AT HYPERSONIC SPEEDS

By John B. McDevitt and Jack A. Mellenthin

Ames Research Center

SUMMARY

A study has been made of the upwash patterns on slender ablating and nonablating cones at angle of attack in the hypersonic flow regime. An oil-film technique was used to display the surface streamlines on the nonablating models and tests were conducted with both laminar and transitional boundary layers. The boundary-layer-edge Mach number and model wall temperature were found to have a strong influence on the magnitude of surface upwash angles. The measured surface upwash angles at small angles of attack agreed well with theoretical estimates in the laminar case. At transitional Reynolds numbers clear evidence was obtained that streamwise vortices are entrained within the boundary layer for cones at angle of attack. The presence of the vortices alters the local heating rates (and shear rates) so that the paths of the vortices are clearly displayed by the oil-film technique. The upward inclination of the vortex paths at angle of attack were found to be considerably less than the inclination of surface streamlines in laminar flow but considerably greater than the upwash inclination at the outer edge of the boundary layer (estimated by a theoretical method-of-characteristics program).

Tests of ablating cones at transitional Reynolds numbers resulted in grooves eroded in the models. These grooves were interpreted to be the result of local increases in heating rates due to vortical disturbances within the boundary layer. The directions of the grooves were essentially the same as those of the vortex paths observed on the nonablating cones under similar test conditions.

INTRODUCTION

The flow near the surface of a slender body in hypersonic flow is characterized by a boundary layer with extreme changes in temperature within the layer. Because of the large temperature recovery near the wall, the fluid density is relatively low and the boundary layer is especially susceptible at hypersonic speeds to cross-flow effects when the body is at angle of attack. Since body viscous and pressure forces are affected by cross flow, primarily through alterations in surface streamline directions and boundary-layer displacement-thickness distribution, a knowledge of the cross-flow phenomena is fundamental to the understanding of hypersonic aerodynamics. Unfortunately, however, the study of cross-flow phenomena has been given relatively little attention in the past. The present report describes the results of a study

of one aspect of cross-flow phenomena, namely, surface upwash patterns on cones, both ablating and nonablating, in hypersonic flow.

The first phase of the study involved the use of an oil-film technique to display the surface streamlines on a series of nonablating cones at various angles of attack. Tests were conducted in both the laminar and transitional flow regimes and the very different flow phenomena that exist for the two regimes are discussed. Measurements of surface upwash angles are compared with theoretical estimates, and the effects of Mach number and wall temperature are discussed. A few tests were also conducted using porous cone models with uniform blowing through the porous surfaces, to determine the effect of mass addition on surface upwash angles. The second part of the study involved tests of ablating cones at angle of attack and the various interesting surface erosion patterns observed are described in this report.

NOTATION

A_b	model base area
E_w	ratio of static enthalpy at model wall to stagnation enthalpy
l	model length
M	Mach number
p_{t_1}	total pressure
T_t	total temperature
T_w	wall temperature
$Re_{\infty,l}, Re_{\infty,x}$	free-stream Reynolds number based on model length or axial station
U	stream velocity
x	axial coordinate of cone model
α	model angle of attack
γ	specific heat ratio
ϵ	upwash angle, measured with respect to the local cone meridian
ϵ_v	upwash angle of mean vortex path

σ_c cone semivertex angle

ϕ cone azimuthal angle, measured with respect to the most windward meridian

$\frac{\dot{m}}{\rho_\infty U_\infty A_b}$ mass addition or ablation rate, normalized by the product of the free-stream density, velocity, and model base area

$\bar{(\ )}$ surface values for cones in invisid flow

$(\ )_\infty$ free-stream values

TESTS AND PROCEDURE

Facilities

The tests were conducted in the Ames 20-Inch Hypersonic Helium Tunnel and in the 3.5-Foot Hypersonic (Air) Tunnel. Both facilities are of the blow-down type, utilizing contoured nozzles to provide nominal Mach numbers of 8, 15, and 20 for the helium tunnel and nominal Mach numbers of 5, 7.5, and 10 for the air tunnel. For the helium tunnel the supply gas is unheated while for the air tunnel the supply gas can be heated to about 1100° K. The test models were sting mounted in the helium facility whereas a "quick-insert" mechanism was used in the air tunnel, which allowed exposure of the model to the hot, hypersonic stream only for the desired time interval.

Models

The test models used for the oil-film studies were solid metal cones with semivertex angles of 5°, 7.5°, 10°, and 15° and porous cones with semivertex angles of 10° and 15° (all the models had base diameters of 3 in.). Each of the porous models (designed for mass addition studies) had a solid portion near the apex, involving the first 15 percent of the cone length, with the remaining portion of the conical surface fabricated from perforated sheet material having 2500 holes (nominally 0.002 in. in diameter) per square inch. For the present tests helium gas was injected through the porous surfaces at a normalized rate of $\dot{m}/\rho_\infty U_\infty A_b = 0.01$. The pressures inside the porous cones were monitored during the tests and it was concluded that the porous surface orifices were operating in a "choked" condition and thus the local surface mass-addition rates were constant and unaffected by changes in model angle of attack.

The ablation test models illustrated in figure 1 were constructed as follows: The model sleeve was placed in a cylindrical mold. Powdered chloride (NH_4Cl) was then added and sintered by compression from a hydraulic piston. The nose spike was then inserted and the final conical shape was machined.

Procedures

The technique for displaying surface flow details on nonablating models consisted of brushing a mixture of vacuum-pump oil and titanium oxide (with a few drops of oleic acid to improve the consistency) on the test model and then blotting the surface, leaving a somewhat mottled appearance. The model was then exposed to the test stream for a suitable interval and the results were recorded by postrun photographs, viewing the model in 45° increments of azimuthal angle.

The ablation models were tested at the highest temperature and pressure levels possible in the air tunnel ($M_\infty = 7.4$, $p_{t_1} = 102$ atm, $T_t \approx 1100°$ K) and various interesting surface erosion patterns were observed. These patterns were also recorded by postrun photographs, and approximate, average ablation rates were obtained by recording the model exposure time and weighing the models before and after the runs.

RESULTS AND DISCUSSION

Oil-Film Studies of Surface Upwash Patterns

The oil-film technique for displaying the streamline patterns on cones was found to be ideally suited for use in heated flow facilities, such as the 3.5-foot tunnel used in the present investigation. After insertion of the model into the test section by the quick-insert mechanism, the hot stream efficiently removes most of the oil mixture but leaves a clear indication of the surface streamline pattern. Application of this technique to tests in the unheated helium facility also used in the present study gave results not nearly so satisfactory, although useful results were obtained. The difficulty encountered in unheated flow facilities stems from the fact that the model wall temperature decreases substantially below the ambient value (the temperature recovery factor in helium at high Mach numbers, for example, is about 0.87 for laminar flow), and the thinning or removal of the oil film depends primarily on shear forces.

In the presentation that follows, the test results obtained in the helium tunnel, confined to measurements where the flow was laminar, are presented first, followed by the air-tunnel results where measurements in both laminar and transitional flow were made.

Measurements in the 20-inch helium tunnel.- Typical photographs of models tested in the helium facility are presented in figure 2; the upper photograph shows a model where the entire forward surface was covered initially with the oil and titanium oxide mixture, whereas for the model shown in the lower photograph, the application of the oil mixture was confined to several narrow circumferential bands. It was found that covering the entire surface is preferable, since, under certain conditions, streamwise vortices

(to be discussed in some detail later in this report) may form in the boundary layer and the presence of these vortices is more easily detected by this technique.

The surface upwash angles, ε, measured from postrun photographs of the test models at axial location x (approximately at midlength), are presented in figure 3 (test results for the most slender cone model, $\sigma_c = 5°$, are not included because of the very poor quality of the measurements). Since the technique as used in the helium facility was not capable of displaying accurately the surface flow details in the transitional flow regime, the measurements presented here are confined to Reynolds numbers where laminar flow existed. (The local boundary-layer-edge Reynolds numbers, which are somewhat higher than the free-stream value quoted in figure 3, can be easily obtained from the theoretical ratios of surface-to-free-stream Reynolds numbers displayed in Chart I.) At small angles of attack (see fig. 3), the maximum upwash angle occurs at the side meridians ($\phi = 90°, 270°$) of the cone and the variation with azimuthal angle can be nicely represented by a $\sin \phi$ variation. As the angle of attack is increased, the variation soon becomes highly unsymmetrical, with the maximum upwash angles occurring at azimuthal angles greater than 90°, and eventually separation of the boundary layer (and possibly the formation of secondary shock waves within the primary shock layer of the cone) occurs; the separation phenomenon appears at a relatively small angle of attack for the most slender cone tested.

For purposes of comparison, calculations were made of upwash angles for cones in inviscid flow (providing an estimate of the flow inclination at the outer edge of the boundary layer) by a "method-of-characteristics" program developed by Rakich (ref. 1) and at the cone surface by the laminar boundary-layer theory of Moore (refs. 2 and 3). The inviscid flow calculations are shown in figure 4 for ideal-gas air ($\gamma = 1.40$) and helium ($\gamma = 1.67$) and are correct only to a first order in angle of attack (note that slender-body theory suggests a value of 2 for the ordinate parameter shown). The theory of Moore, which assumes an insulated wall and is also correct only to a first order in angle of attack, predicts the upwash to be

$$\frac{\varepsilon}{\alpha \sin \phi} = \varepsilon_{\text{inviscid}} \left[1 + 1.3 \left(1 + \frac{\gamma - 1}{2} \overline{M}^2\right)\right] \tag{1}$$

Calculations for both air and helium are presented in figure 5. Whereas the ratio of inviscid upwash angle to cone angle of attack is small (less than unity at high Mach numbers, fig. 4) and decreases with increasing Mach number, the surface upwash in the viscous case is a strong function of the cone edge Mach number and can be an order of magnitude greater than the angle of attack for slender cones at high Mach numbers, as indicated in figure 5.

The measured upwash angles at the side meridians of the three cones tested are compared with theoretical estimates in figure 6. The experimental

values agree remarkably well with Moore's theory for very small angles of attack but the experimental values show a nonlinear variation with angle of attack, and the agreement between linear theory and experiment deteriorates rapidly with increasing angle of attack.

In a few test runs using porous cone models, ambient helium was injected through the porous surfaces at a normalized mass addition rate of $\dot{m}/\rho_\infty U_\infty A_b = 0.01$ (the oil film was applied in narrow bands, similar to the example shown in the lower photograph of fig. 2). The results are summarized in figure 7. The effect of mass addition was small; the differences indicated in figure 7 are probably within the overall accuracy of the tests.

Measurements in the 3.5-foot hypersonic air tunnel.- A typical photograph illustrating the oil-film technique for displaying the laminar upwash at the surface of a cone in the heated air tunnel is presented in figure 8. The measured upwash angles for tests conducted at a tunnel total pressure of 34 atm are presented in figure 9. For these tests the boundary layers were believed to be laminar in all cases, at least for small angles of attack, and the upwash angles did not appear to be sensitive to axial location (i.e., were not dependent on Reynolds number). The general appearance of the data is similar to that observed in the helium-tunnel tests; that is, for small angles of attack the upwash varies approximately as $\sin \phi$, but as the angle of attack is increased, the location of maximum upwash inclination shifts around the cone to azimuthal angles considerably greater than 90°, and flow separation eventually occurs on the leeward side. However, in the present case separation is delayed to much higher angles of attack, probably because of the much thinner boundary layers present and the influence of the cold wall on stream density.

A comparison of theory and experiment is also of interest here. The inviscid predictions presented for air in figure 4 also apply here (the wall condition does not enter into consideration for the inviscid case). Although Moore's predictions for upwash angles (see fig. 5) apply only for the insulated wall case, the results may also be used in the "cold wall" case by employing a correction factor derived from Beckwith's similarity solutions for small cross flows (ref. 4). The effect of changes in flow enthalpy at the wall on upwash angles for cones may be evaluated by comparison of the solutions presented in reference 4 for the zero pressure gradient case ($\beta = 0$). The result is the correction factor shown in figure 10, where E_w is the ratio of static enthalpy at the wall to stagnation enthalpy. A comparison of measured and theoretical upwash angles at the side meridian of the cones is presented in figure 11. (The theoretical values were obtained by reducing Moore's predictions according to figure 10, the reduction in the present case being about 50 percent.) The agreement between experiment and modified theory is excellent for small angles of attack (it should be recalled that Moore's analysis considered only first-order α effects).

The experimental measurements just described were obtained by operating the tunnel at a total pressure of 34 atm. A few additional tests were conducted at the highest total pressure (102 atm) permissible for this facility when the "M = 7.5" nozzle is used. Typical photographs obtained during the

high Reynolds number tests are presented in figures 12 and 13 for cones having semivertex angles of 10° and 15°, both tested at an angle of attack of 5°. Near the apex of the models the appearance of the upwash pattern is similar to that obtained previously and the upwash angles also agree well with previous measurements. However, on the aft, leeward portions of the models evidence of the existence of streamwise vortices entrained within the boundary layer is apparent (see enlarged view of leeward surface in fig. 14). Since the vortices increase local heating rates and shear forces, the result is that the vortex paths are prominently displayed by the oil-film technique. The presence of the vortices, of course, alters the velocity profiles in the boundary layer and the simple spiral-like pattern of surface streamlines in the laminar case is replaced by an intricate pattern reflecting the interaction between the vortices and the cross flow.

The upward inclinations of the vortex paths at the side meridians of the cones were measured from the photographs; they are compared in figure 15 with surface upwash angles measured near the apex of the models where the flow appeared to be laminar, and with theoretical upwash angles estimated for inviscid flow. The inclination of the vortex paths, although much less than that for the surface streamlines in laminar flow, is noticeably greater than the inviscid predictions (i.e., the upwash at the outer edge of the boundary layer), which substantiates the argument that the vortices are entrained (at least initially) within the boundary layer.

No vortices were indicated by the oil-film technique on either the $\sigma_c = 10°$ or 15° model at $\alpha = 0°$; however, there was evidence of vortices near the leeward surface at $\alpha = 4°$, and at larger angles of attack it was clear that an orderly array of more or less regularly spaced vortices surrounded the cone, except in the immediate vicinity of the windward stagnation line.

Ablation Tests

Photographs of the ammonium-chloride ablation models, tested at zero angle of attack, are presented in figure 16 and photographs of models tested at angles of attack of 5° and 10° are presented in figures 17 through 20. (The tests were conducted at a free-stream Mach number of 7.4, total pressure of 102 atm, and total temperature of 1100° K, and the models were exposed to the hypersonic stream for about 60 sec.)

At zero angle of attack, longitudinal grooves, the result of streamwise vortices intensifying the local heating rates (and shear forces), were eroded in the surface of the 15° half-angle cone, but these grooves were not present on the more slender cone (see fig. 16). In the oil-film study of similar but nonablating cones at identical test conditions, streamwise vortices did not appear to be present at $\alpha = 0°$. For the ablating models the local heating and ablation rates are most severe just downstream of the metal nose tip, resulting in a rearward facing step and a concave cavity which provide a source for longitudinal curvature to the streamline and probably enhance the formation of vortices (see discussion in ref. 5).

At angle of attack (see figs. 17 through 20), upwash groove patterns were eroded in all of the models, and in one case (the larger angle cone at $\alpha = 10°$) a cross-hatching pattern appeared but was confined to the windward side.

Since the ablated grooves are believed to be the result of the same basic phenomena as the vortex paths observed by the oil-film technique on nonablating models at the same test conditions, it would be interesting to compare the cross-flow inclination angles involved. Such a comparison is made in figure 21 which indicates that the upwash inclinations are the same within the accuracy limits of the tests.

CONCLUDING REMARKS

This application of the oil-film technique for displaying surface streamlines on test models has demonstrated that the inclination of surface upwash on cones at angle of attack in laminar flow is strongly dependent on local Mach number and wall temperature. The measured upwash angles at small angles of attack were found to agree well with the laminar boundary-layer theory of Moore for the adiabatic wall case. For a "cold-wall" case good agreement between theory and experiment was also obtained at small angles of attack when Moore's theory was adjusted to account for the nonadiabatic wall condition by employing a correction factor obtained from theoretical work by Beckwith.

The application of the oil-film technique at transitional Reynolds numbers led to clear evidence that streamwise vortices are entrained within the boundary layer for cones at angle of attack. The paths of the vortices were prominently displayed by the oil-film experimental technique used, and it was found that the upward inclination of the vortices was considerably less than the inclination of surface streamlines in laminar flow but considerably greater than the upwash at the outer edge of the boundary layer (estimated by a method-of-characteristics program).

Tests of ablating cones at transitional Reynolds numbers resulted in upwash groove patterns eroded in the model surfaces. These grooves were interpreted to be the result of vortices intensifying local heating rates. The upward inclination of the grooves agreed closely with the inclination of the vortex paths measured on the nonablating cones under similar test conditions.

Ames Research Center
National Aeronautics and Space Administration
Moffett Field, Calif. 94035, May 1, 1969

REFERENCES

1. Rakich, John V.: Numerical Calculation of Supersonic Flows of a Perfect Gas Over Bodies of Revolution at Small Angles of Yaw. NASA TN D-2390, 1964.

2. Moore, Franklin K.: Laminar Boundary Layer on a Circular Cone in Supersonic Flow at a Small Angle of Attack. NACA TN 2521, 1951.

3. Moore, Franklin K.: Displacement Effect of a Three-Dimensional Boundary Layer. NACA TN 2722, 1952.

4. Beckwith, Ivan E.: Similarity Solutions for Small Cross Flows in Laminar Compressible Boundary Layers. NASA TR R-107, 1961.

5. Tobak, Murray: Hypothesis for the Origin of Cross-Hatching. AIAA Paper 69-11, 1969.

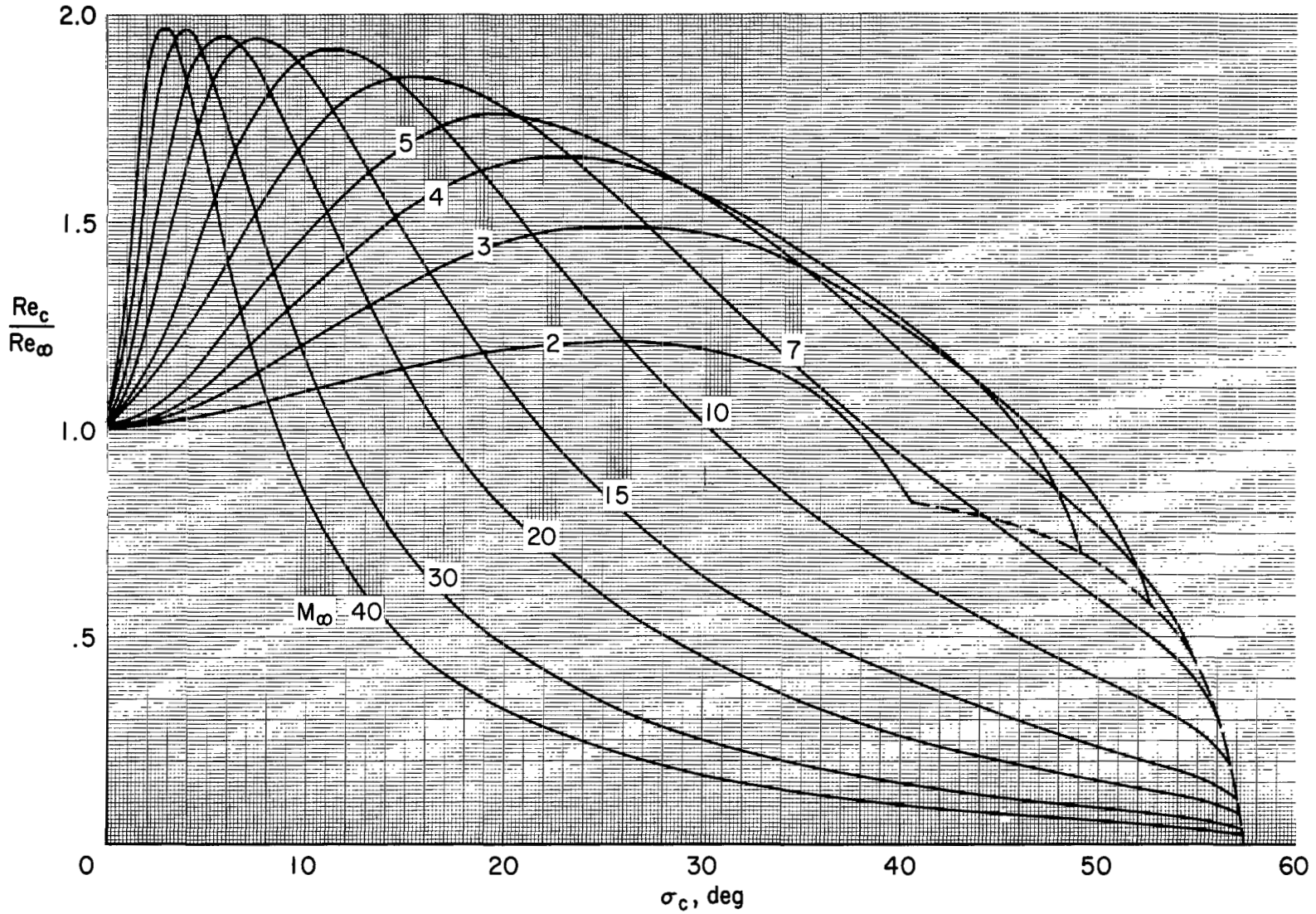

(a) Air (γ = 1.40)

Chart I.- Ratio of inviscid Reynolds number at cone surface to free-stream Reynolds number.

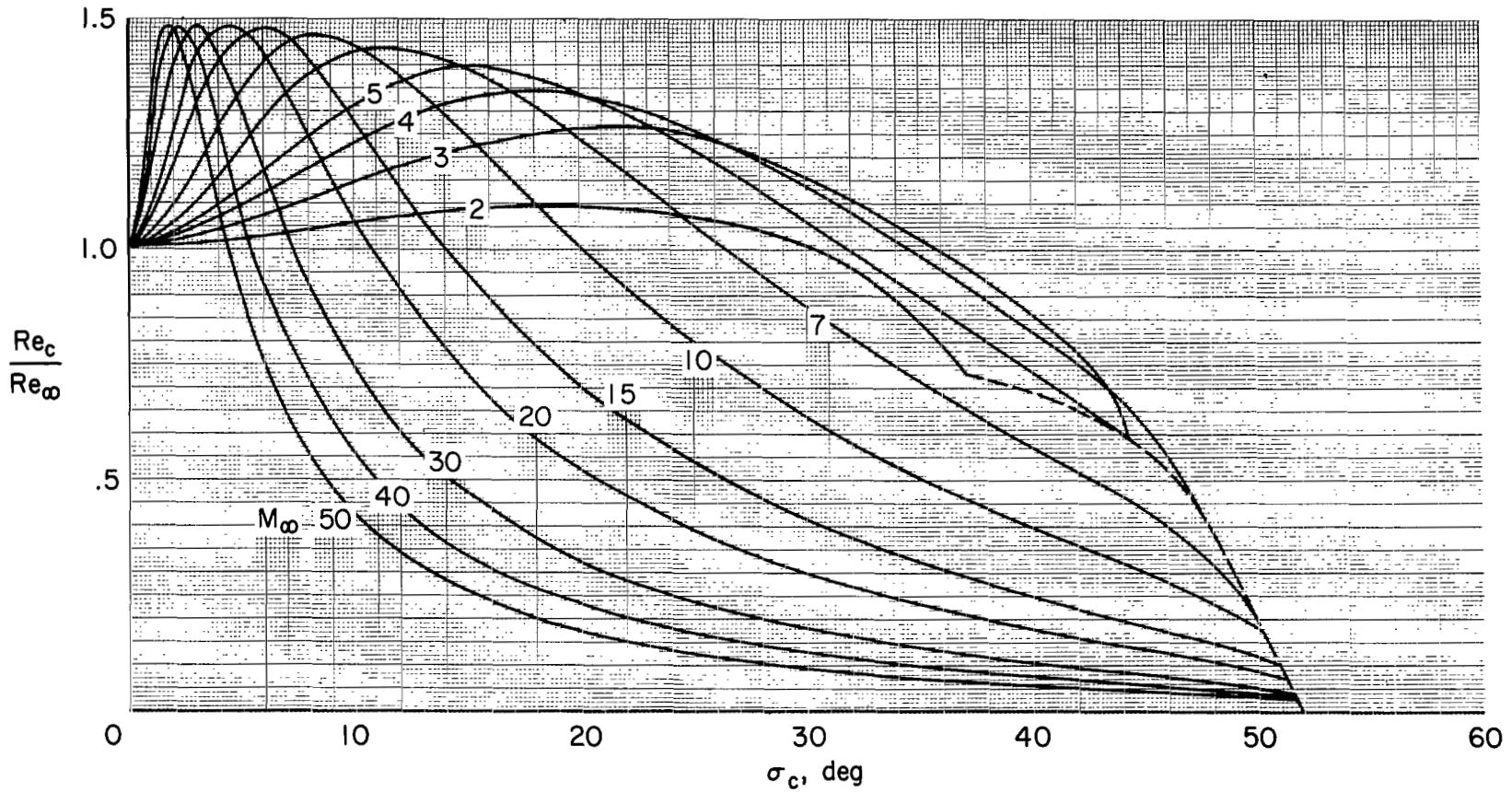

(b) Helium (γ = 1.67)

Chart I.- Concluded.

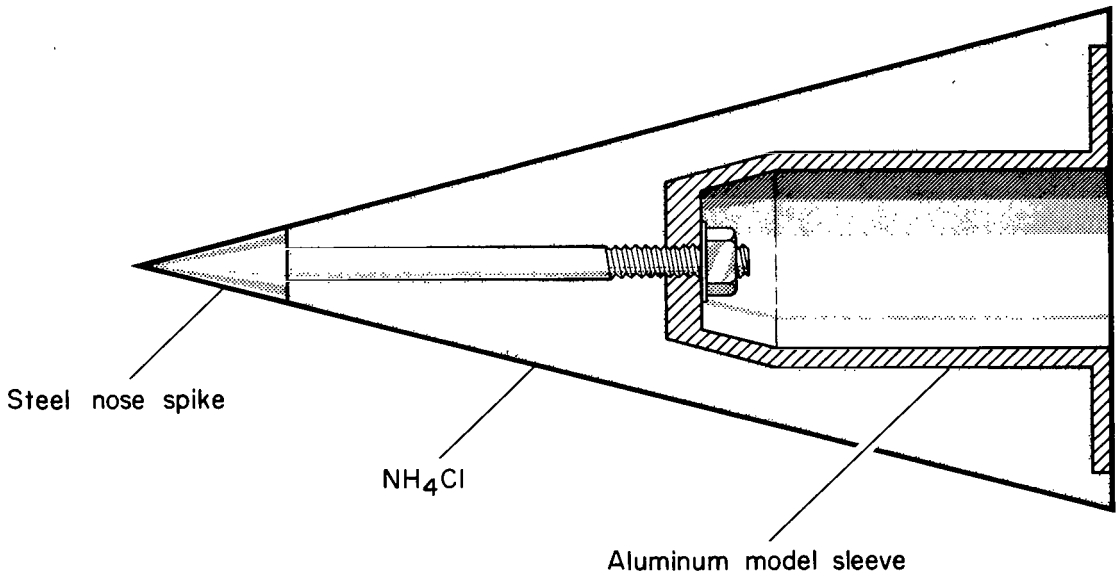

Figure 1.- Sketch of ablation test models.

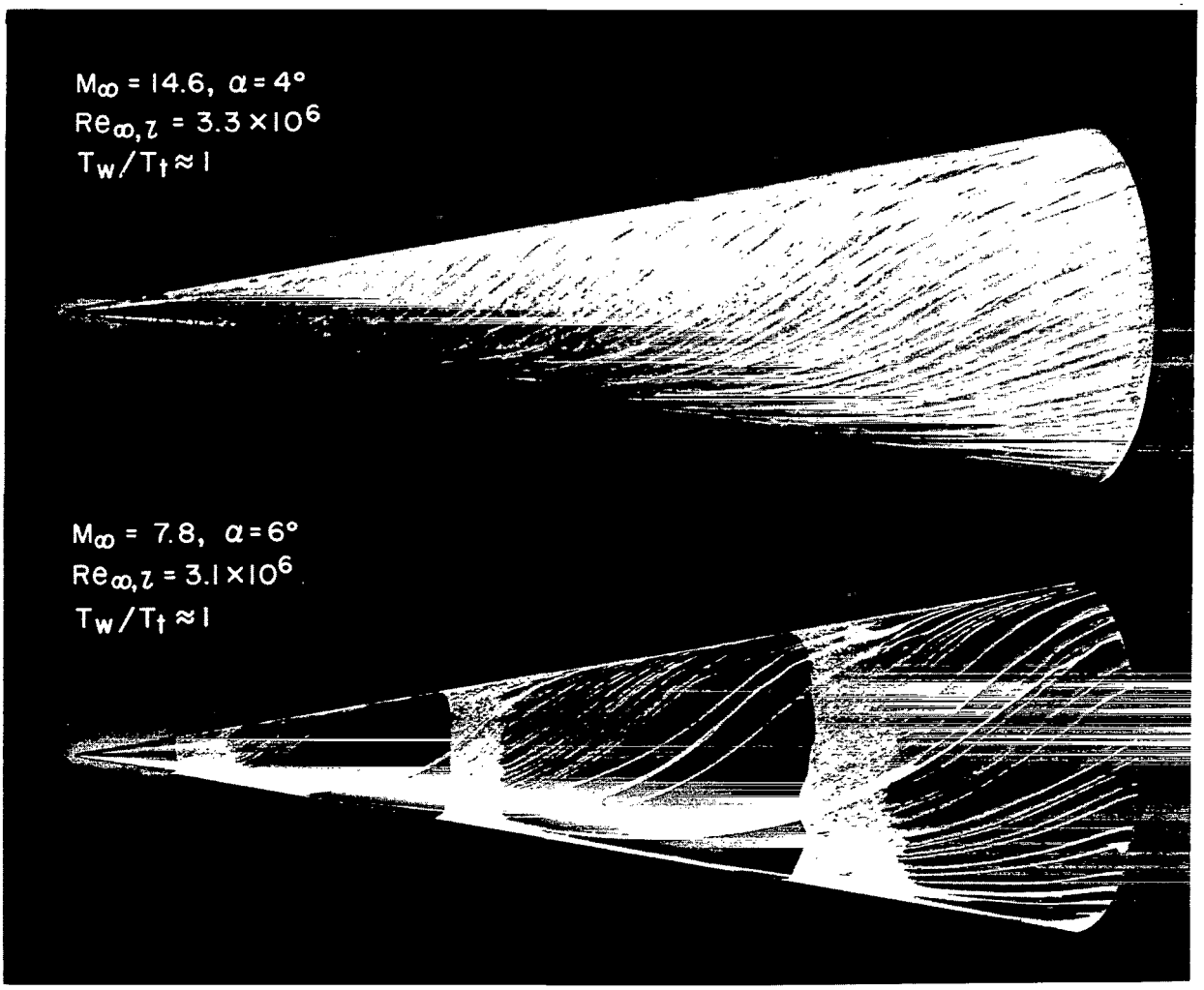

Figure 2.- Typical photographs of 10° half-angle cones with surface streamlines made visible by the oil-film technique, helium flow.

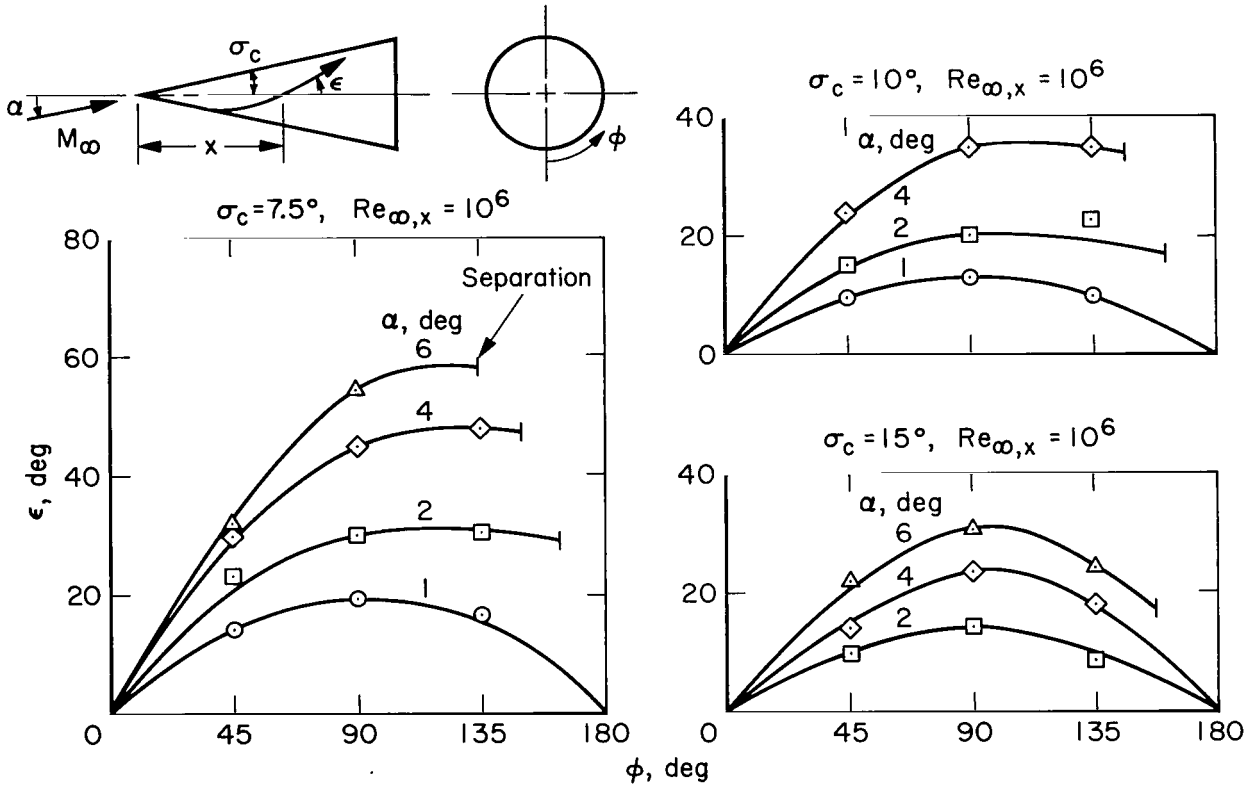

Figure 3.- Measured upwash angles on nonablating cones in helium; M_∞ = 14.6; oil-film technique, $T_w/T_t \approx 1$.

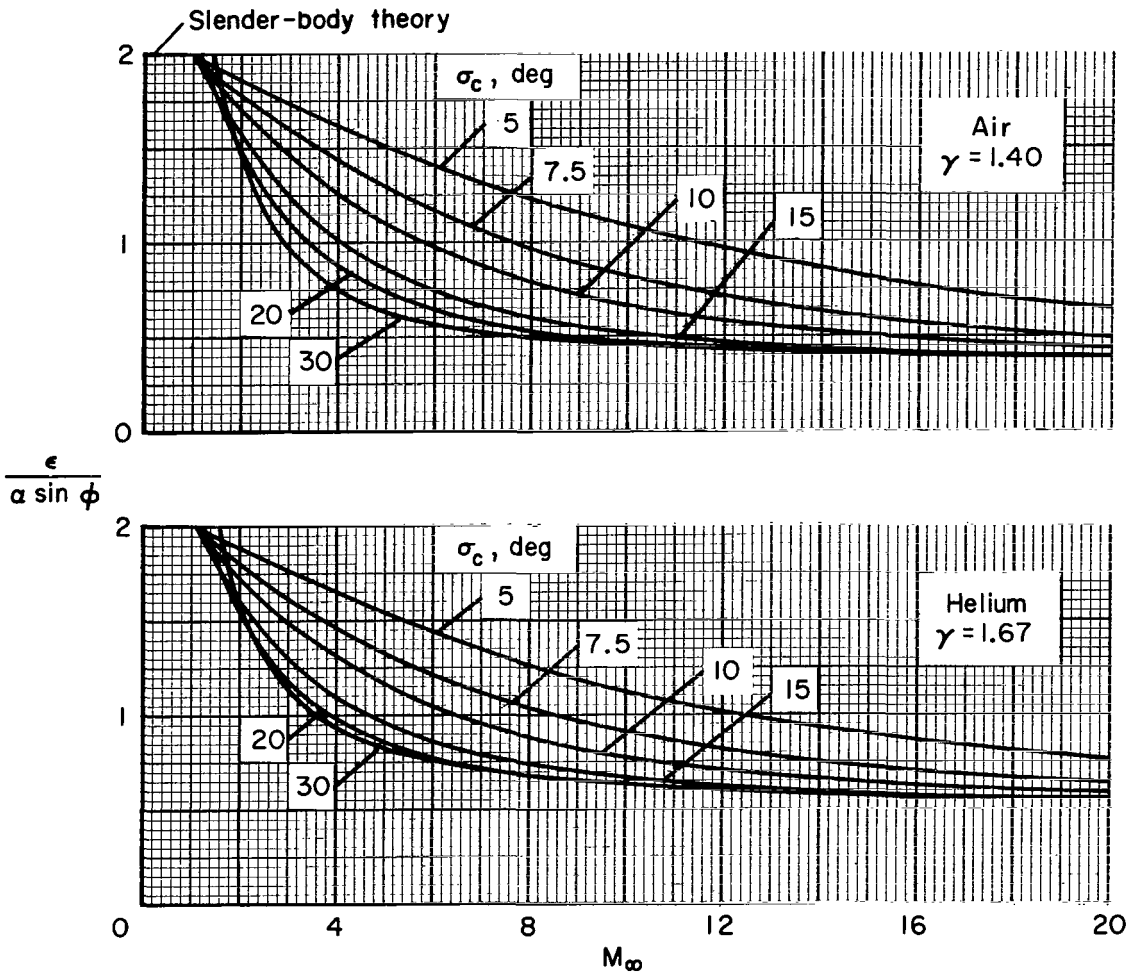

Figure 4.- Theoretical values of surface upwash for cones at small angles of attack in inviscid flow.

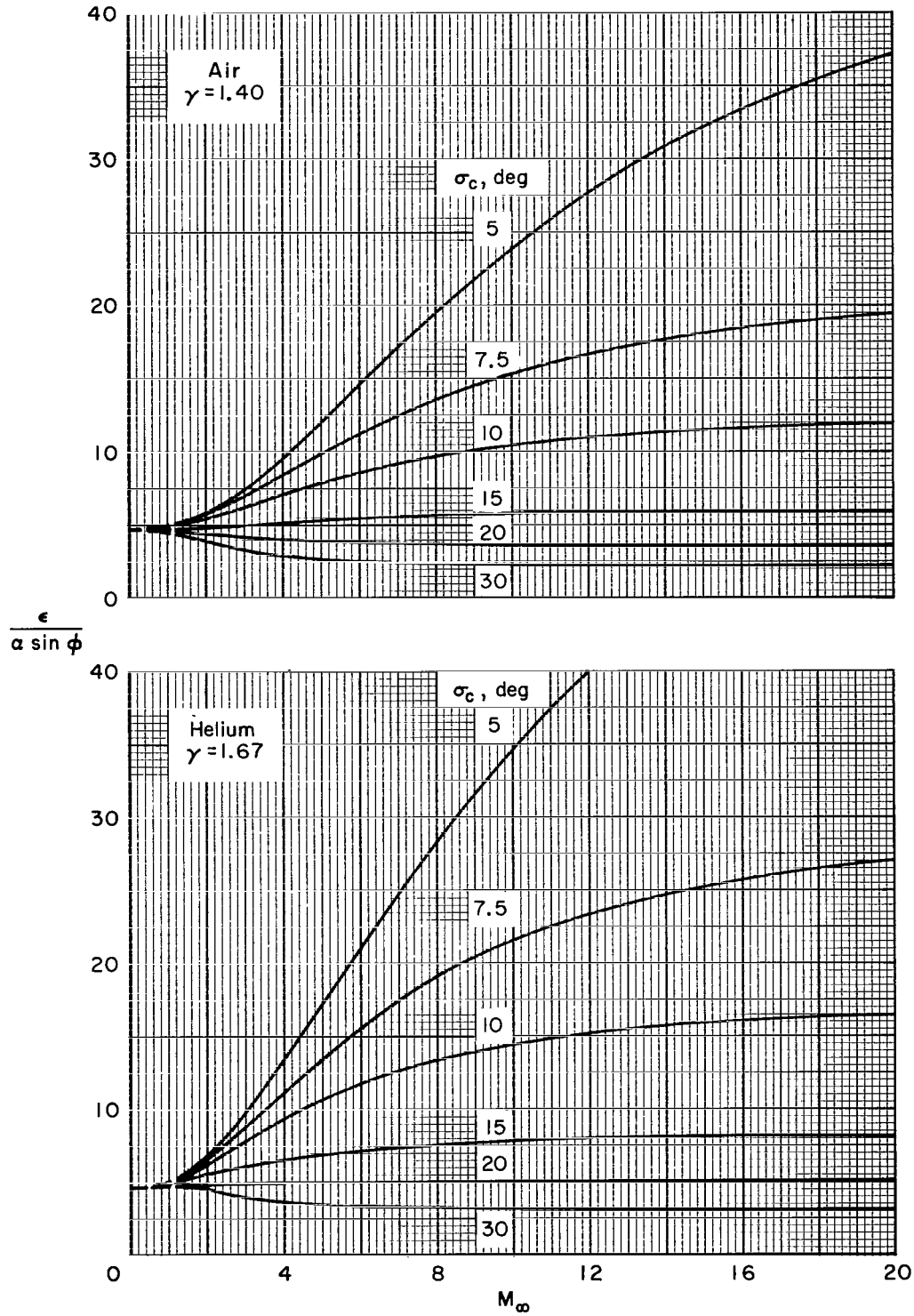

Figure 5.- Theoretical values of surface upwash for cones at small angles of attack with a laminar boundary layer and adiabatic wall.

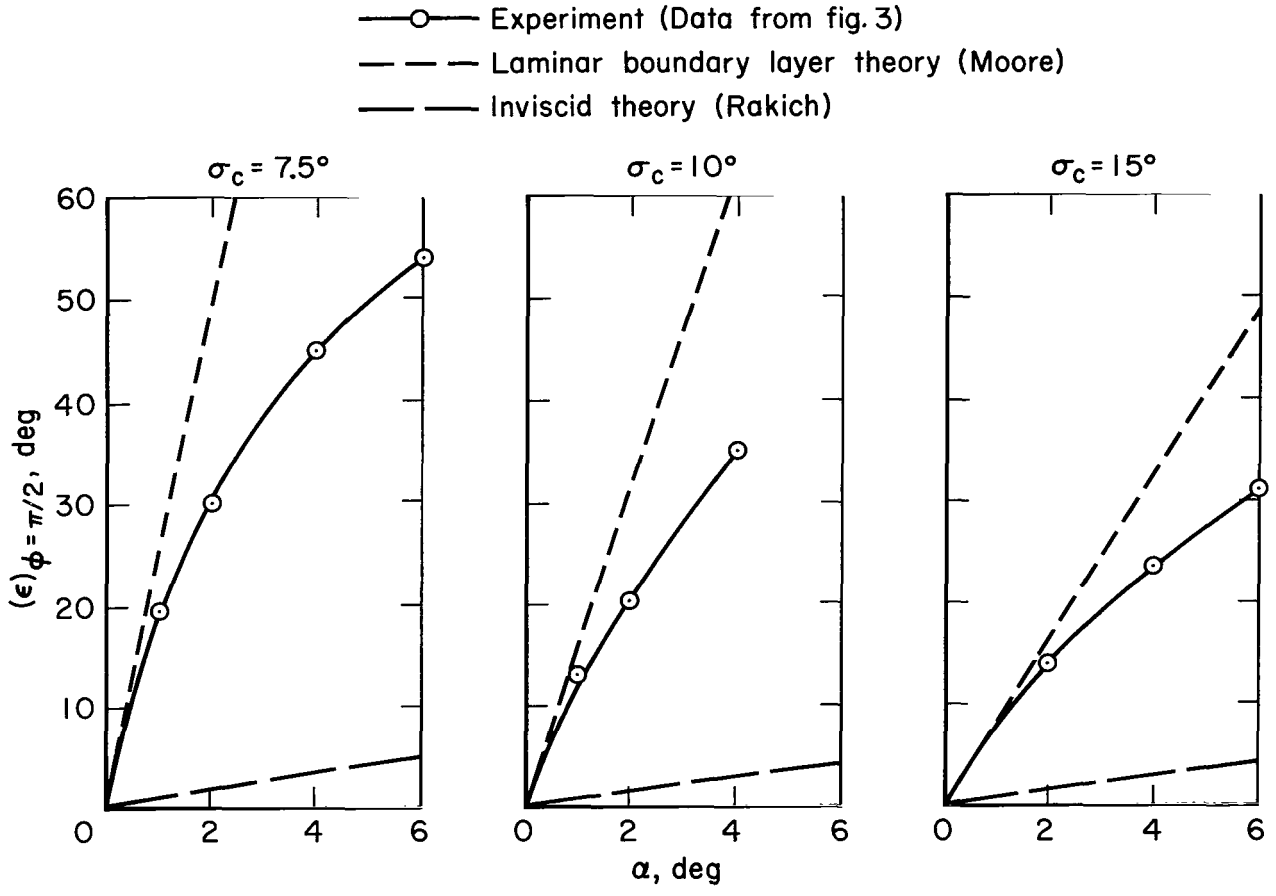

Figure 6.- Comparison of upwash measurements with theory; M_∞ = 14.6 (helium), adiabatic wall.

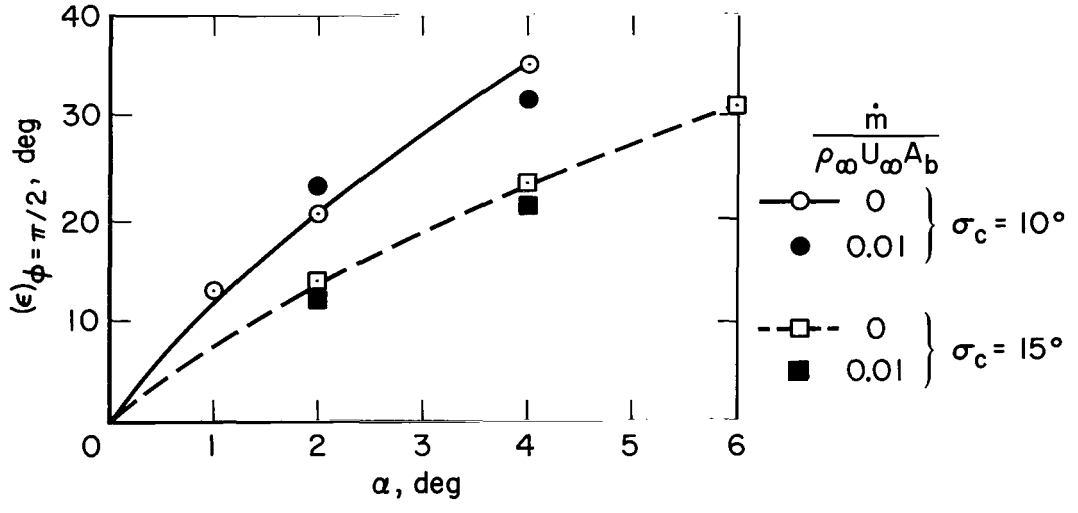

Figure 7.- Effect of mass addition (uniform blowing) on surface upwash angles; M_∞ = 14.6 (helium), $Re_{\infty,x} = 10^6$, $T_w/T_t \approx 1$.

Figure 8.- Typical photograph of surface streamlines on a 10° half-angle cone with laminar flow in air.

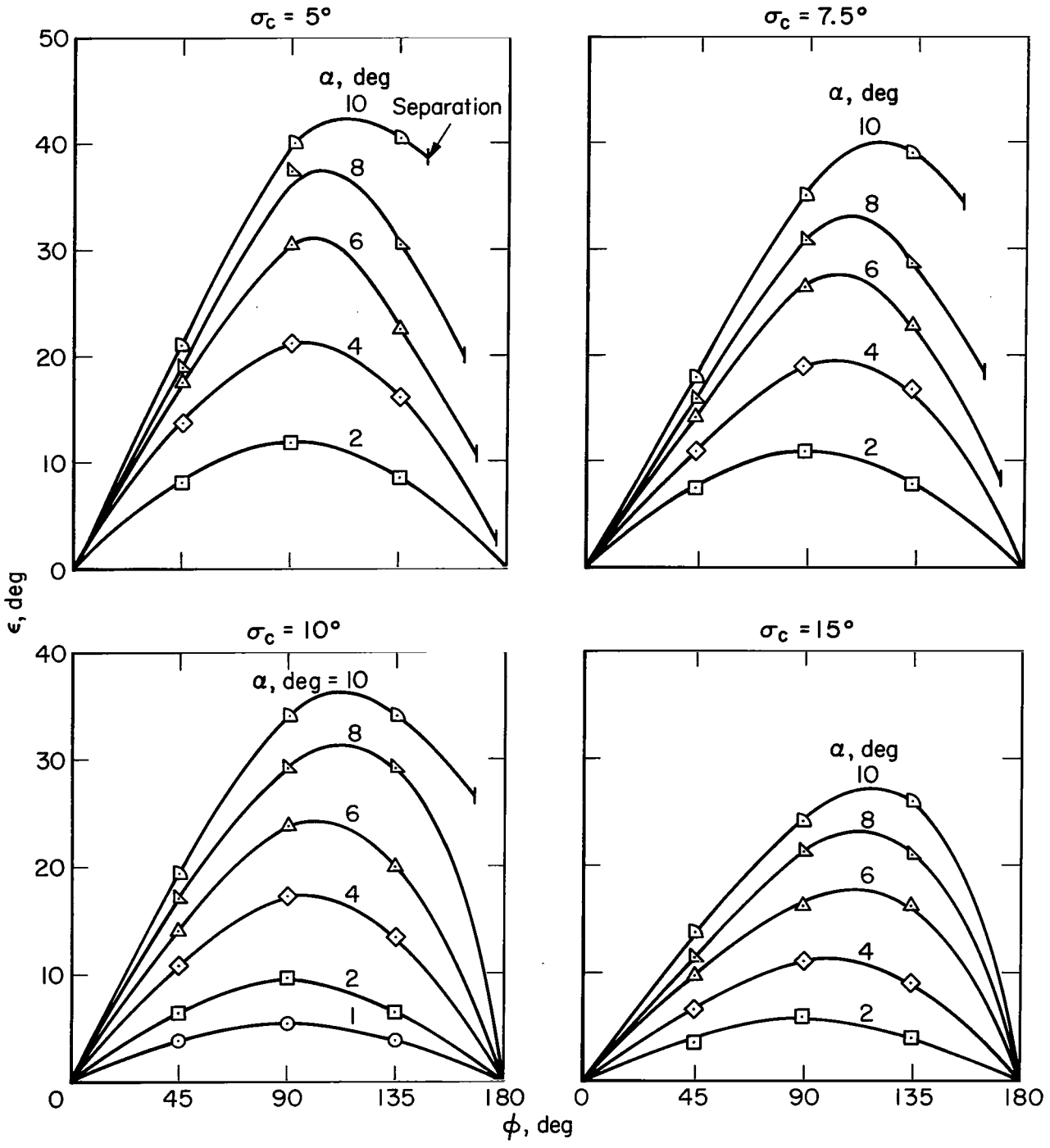

Figure 9.- Measured upwash angles on nonablating cones in air; oil-film technique; M_∞ = 7.4, $Re_{\infty,x}$ = 0.5×10^6, $T_w/T_t \approx 0.3$.

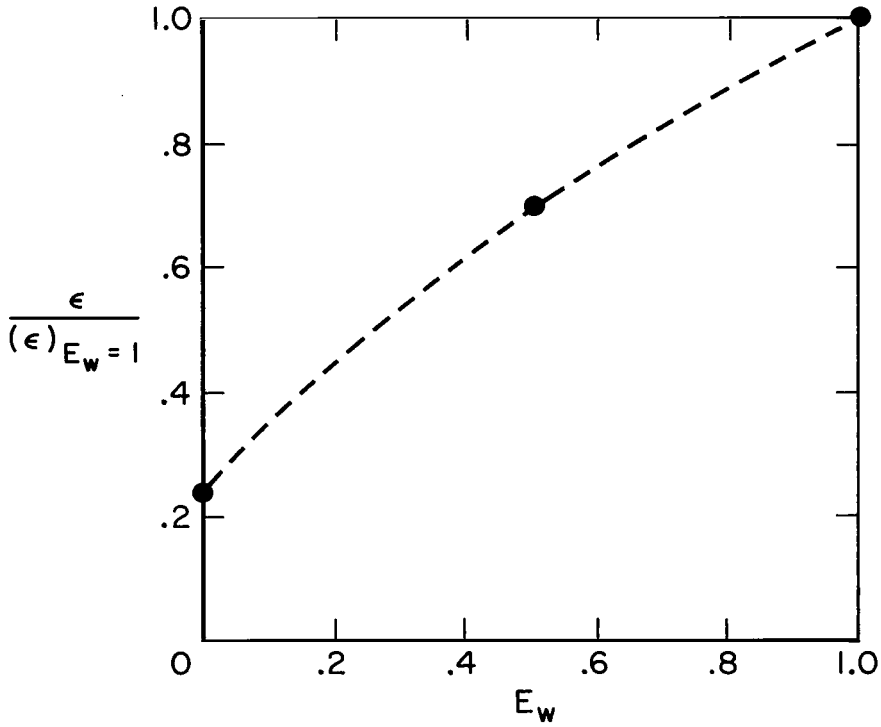

Figure 10.- Effect of enthalpy ratio (ratio of static enthalpy at the wall to stagnation enthalpy) on surface upwash angle.

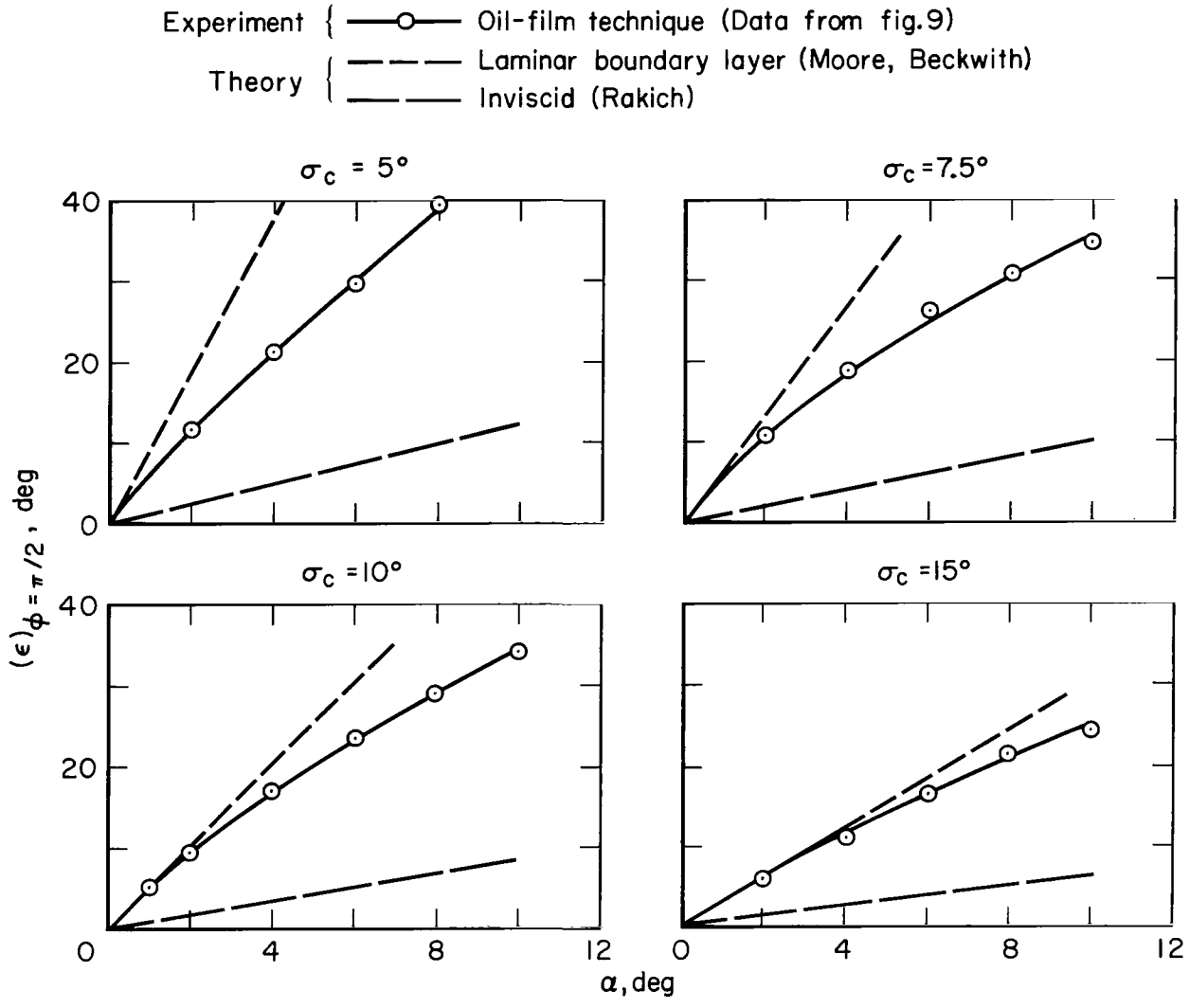

Figure 11.- Comparison of upwash measurements with theory; M_∞ = 7.4 (air), cold wall ($T_w/T_t \approx 0.3$).

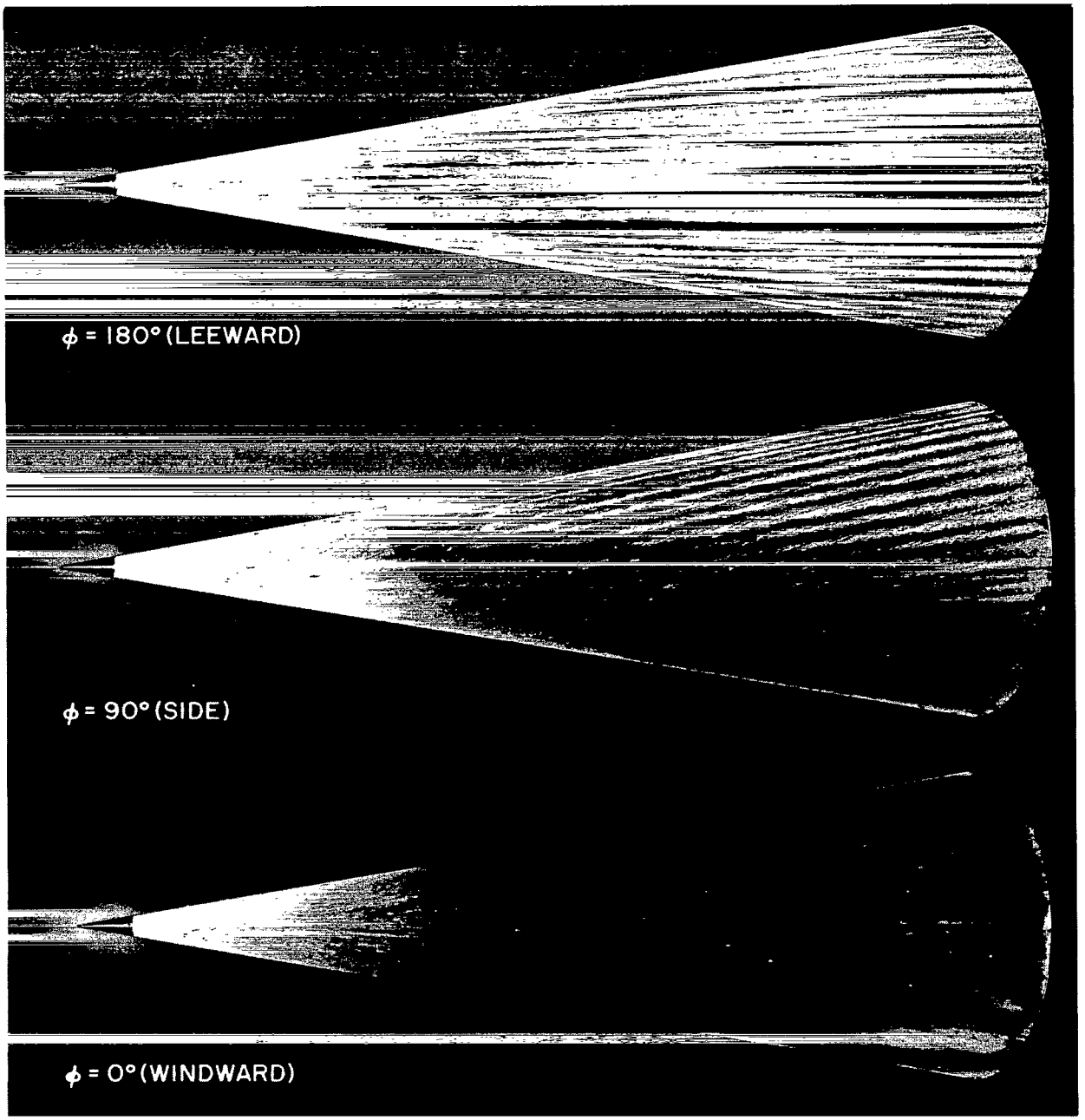

Figure 12.- Oil-film study of a 10° half-angle cone at 5° angle of attack with transitional boundary layer; M_∞ = 7.4 (air), $Re_{\infty,l}$ = 3×10^6, T_t = 1050° K.

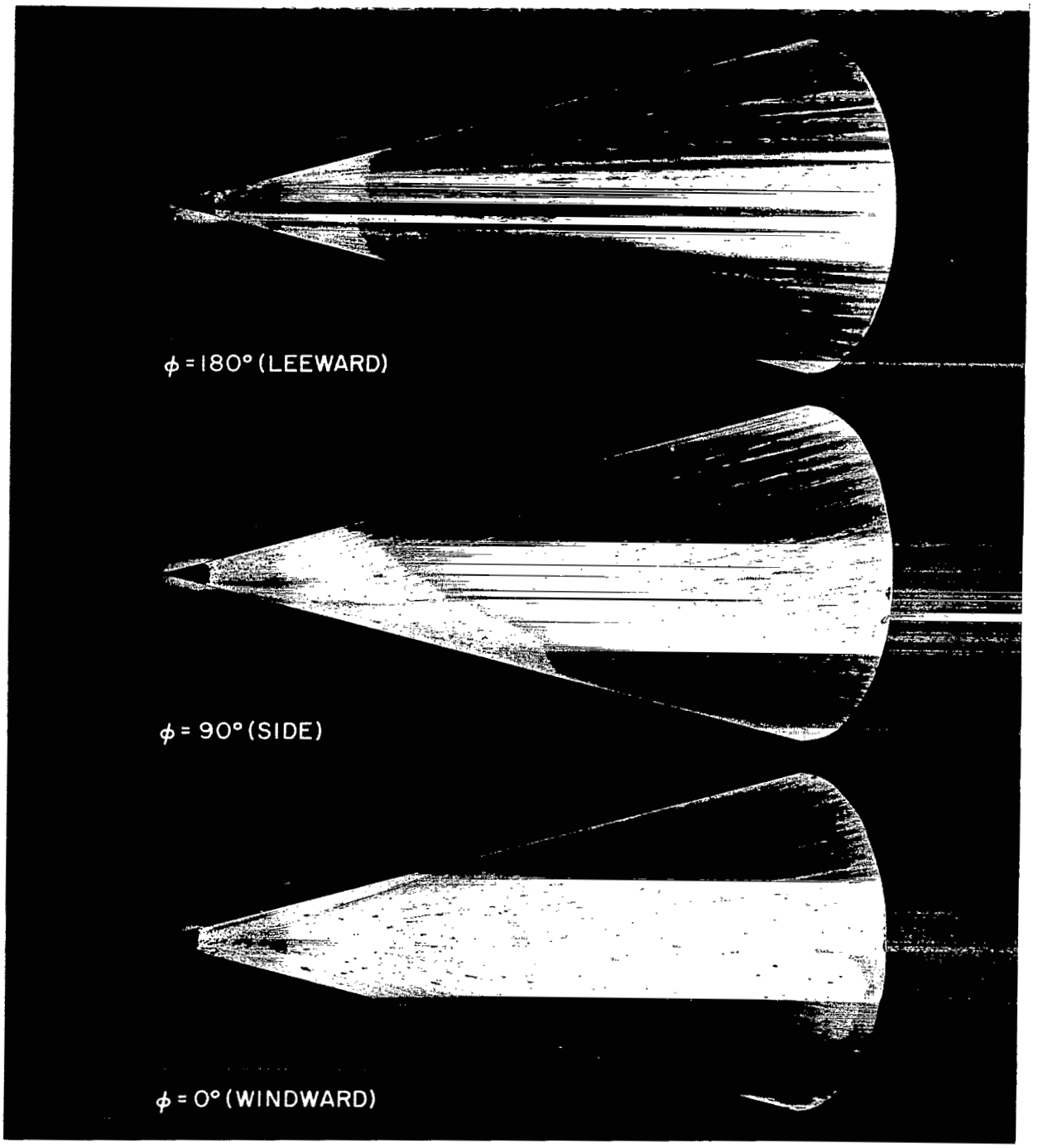

Figure 13.- Oil-film study of a 15° half-angle cone at 5° angle of attack with transitional boundary layer; M_∞ = 7.4 (air), $Re_{\infty,l}$ = 3×10^6, T_t = 1050° K.

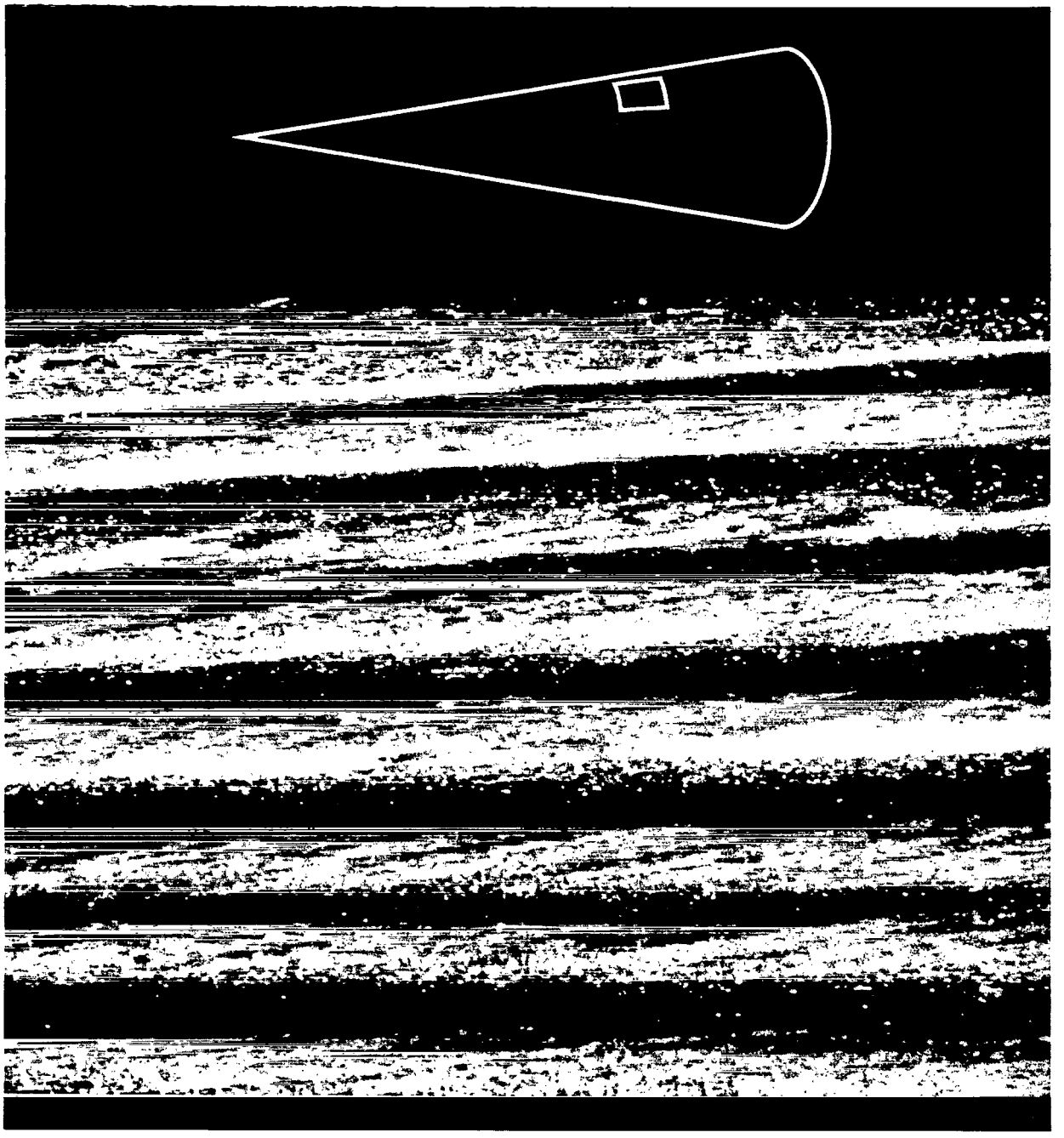

Figure 14.- Enlarged view of a portion of the leeward surface ($\phi \approx 135°$, $x/\ell \approx 0.7$) of the oil-film test model shown in figure 12.

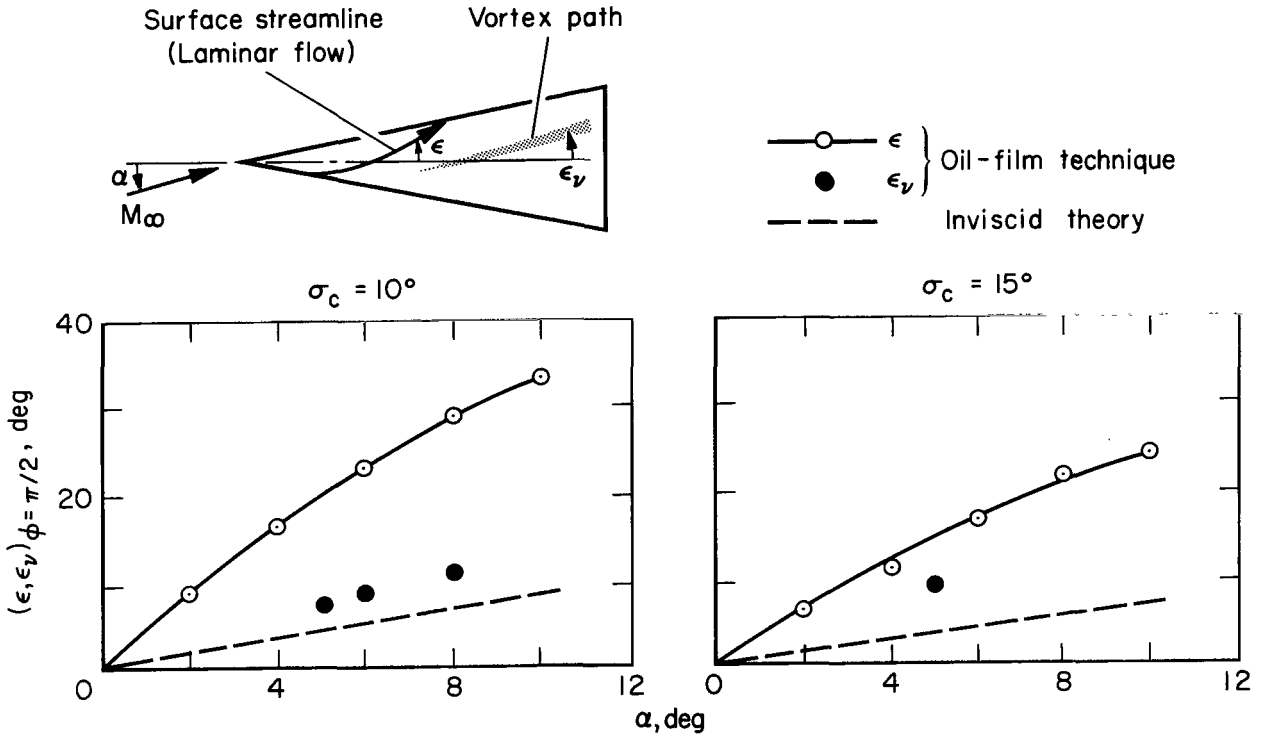

Figure 15.- Inclination of vortex paths at cone side meridians; M_∞ = 7.4 (air), $Re_{\infty,\ell} = 3\times10^6$.

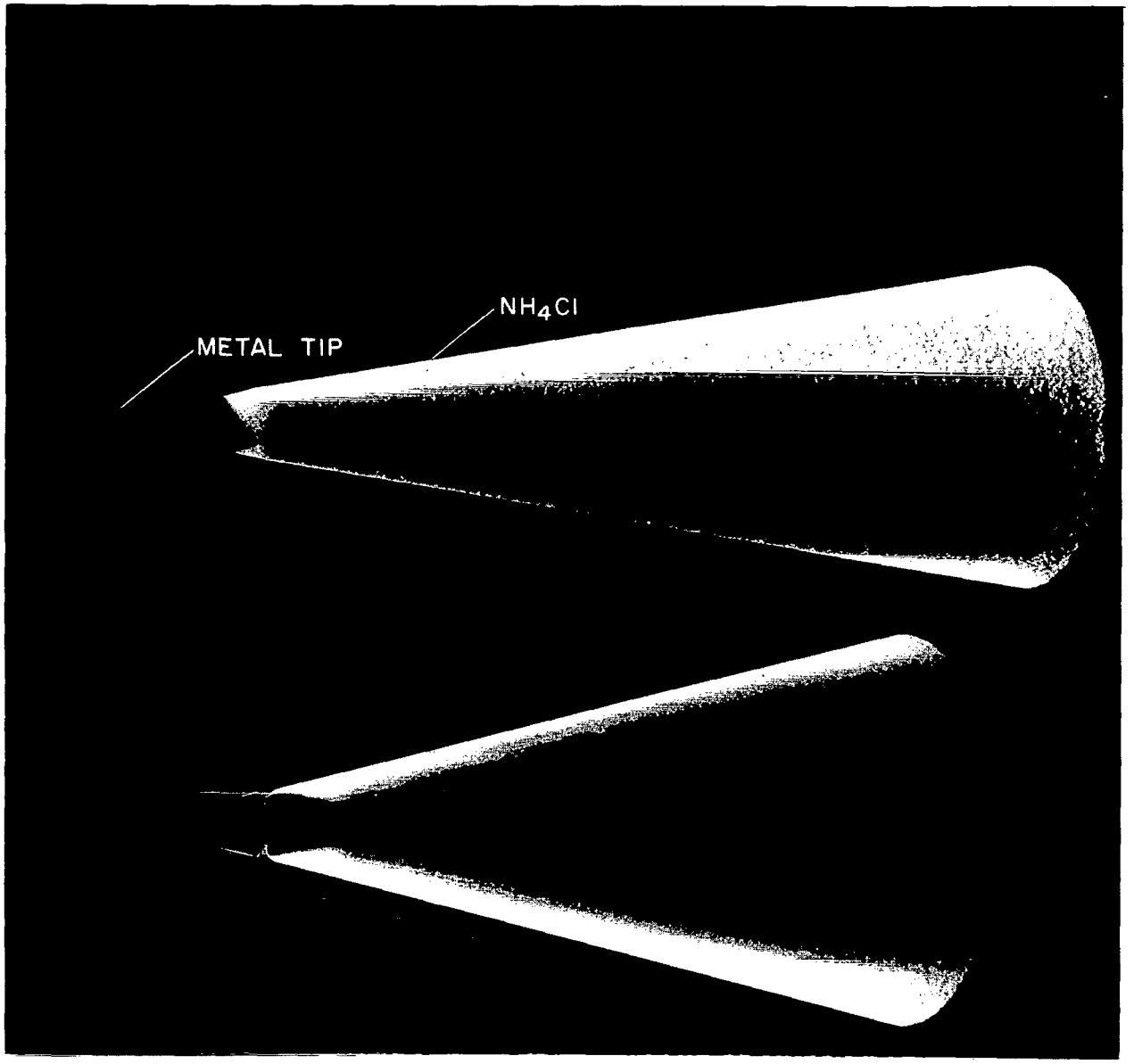

Figure 16.- Photographs of 10° and 15° half-angle ammonium chloride cones tested at zero angle of attack; $M_\infty = 7.4$, $Re_{\infty,\ell} = 3\times10^6$.

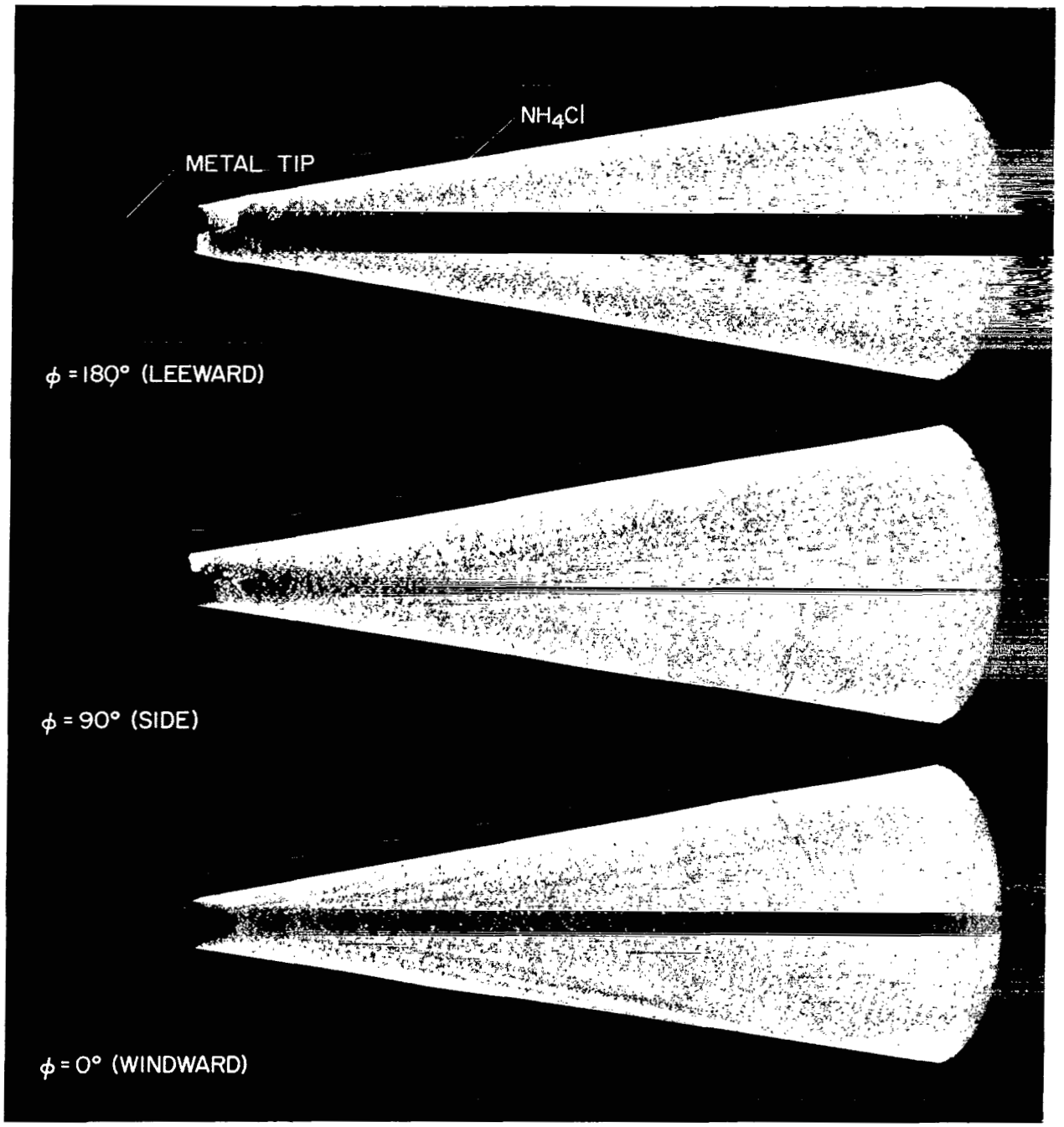

Figure 17.- Photographs of a 10° half-angle cone tested at an angle of attack of 5°; $M_\infty = 7.4$, $Re_{\infty,l} = 3\times10^6$, $\dot{m}/\rho_\infty U_\infty A_b \approx 0.0007$.

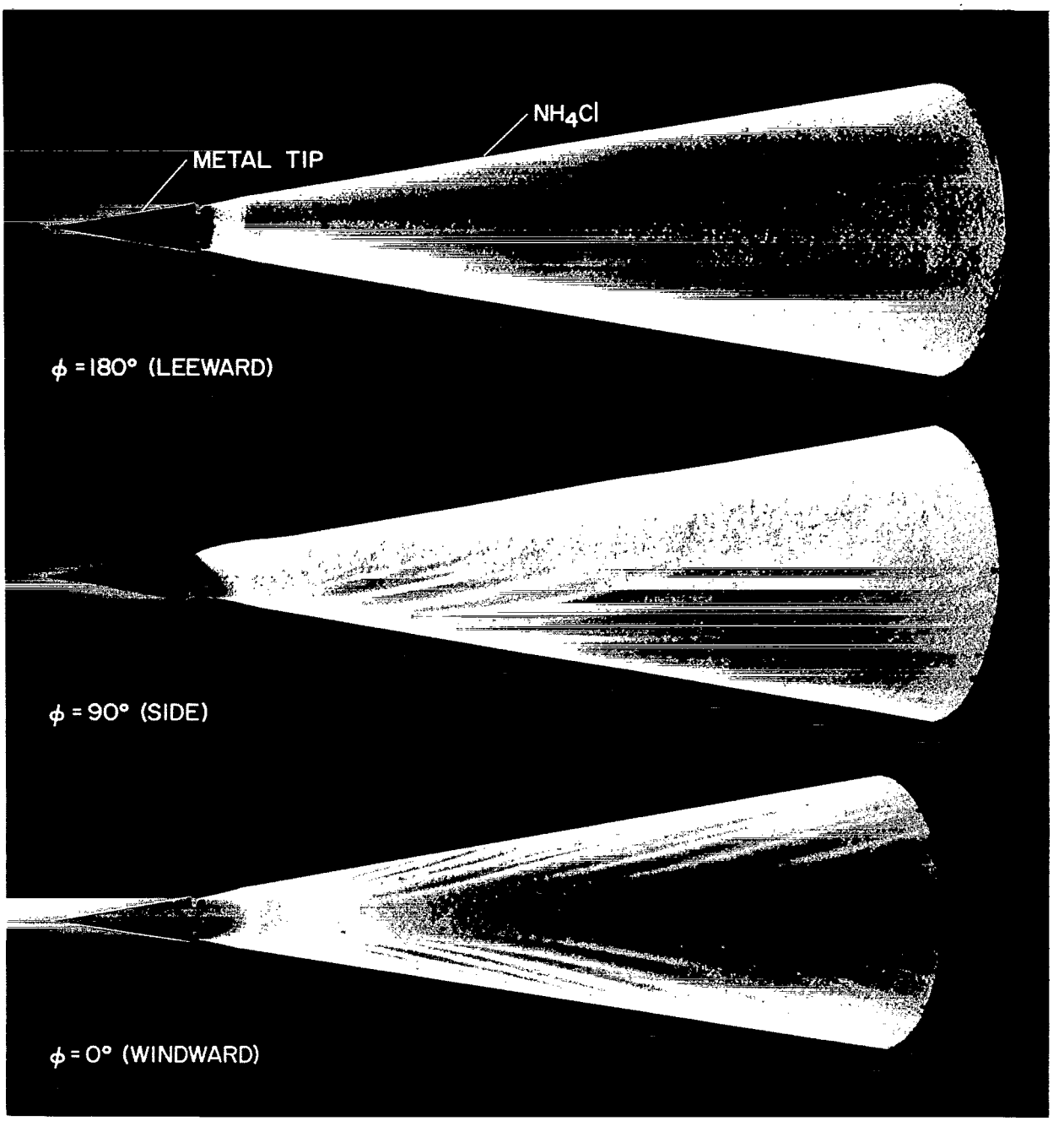

Figure 18.- Photographs of a 10° half-angle cone tested at an angle of attack of 10°; $M_\infty = 7.4$, $Re_{\infty,\ell} = 3\times10^6$, $\dot{m}/\rho_\infty U_\infty A_b \approx 0.0007$.

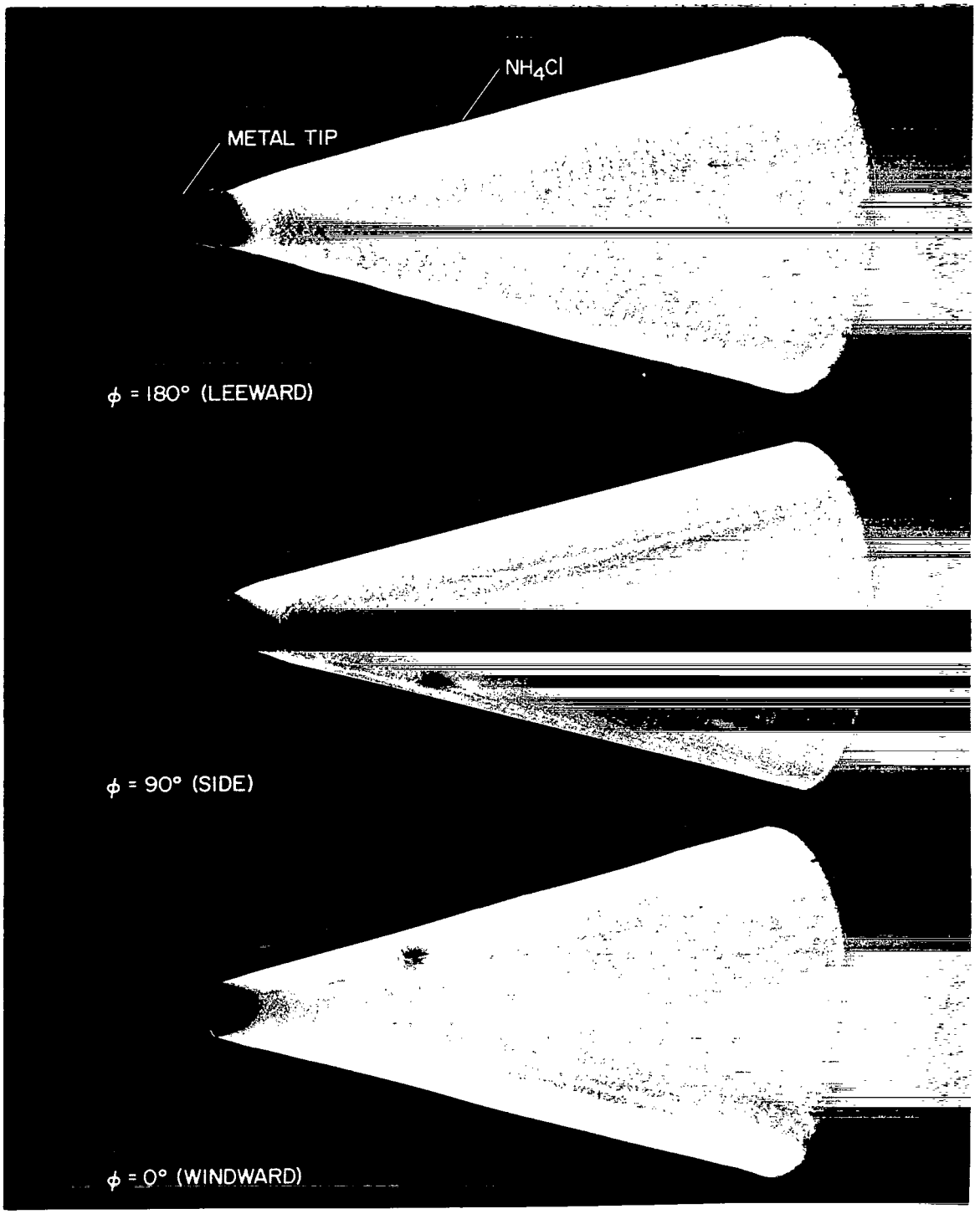

Figure 19.- Photographs of a 15° half-angle cone tested at an angle of attack of 5°; $M_\infty = 7.4$, $Re_{\infty,l} = 3\times10^6$, $\dot{m}/\rho_\infty U_\infty A_b \approx 0.0006$.

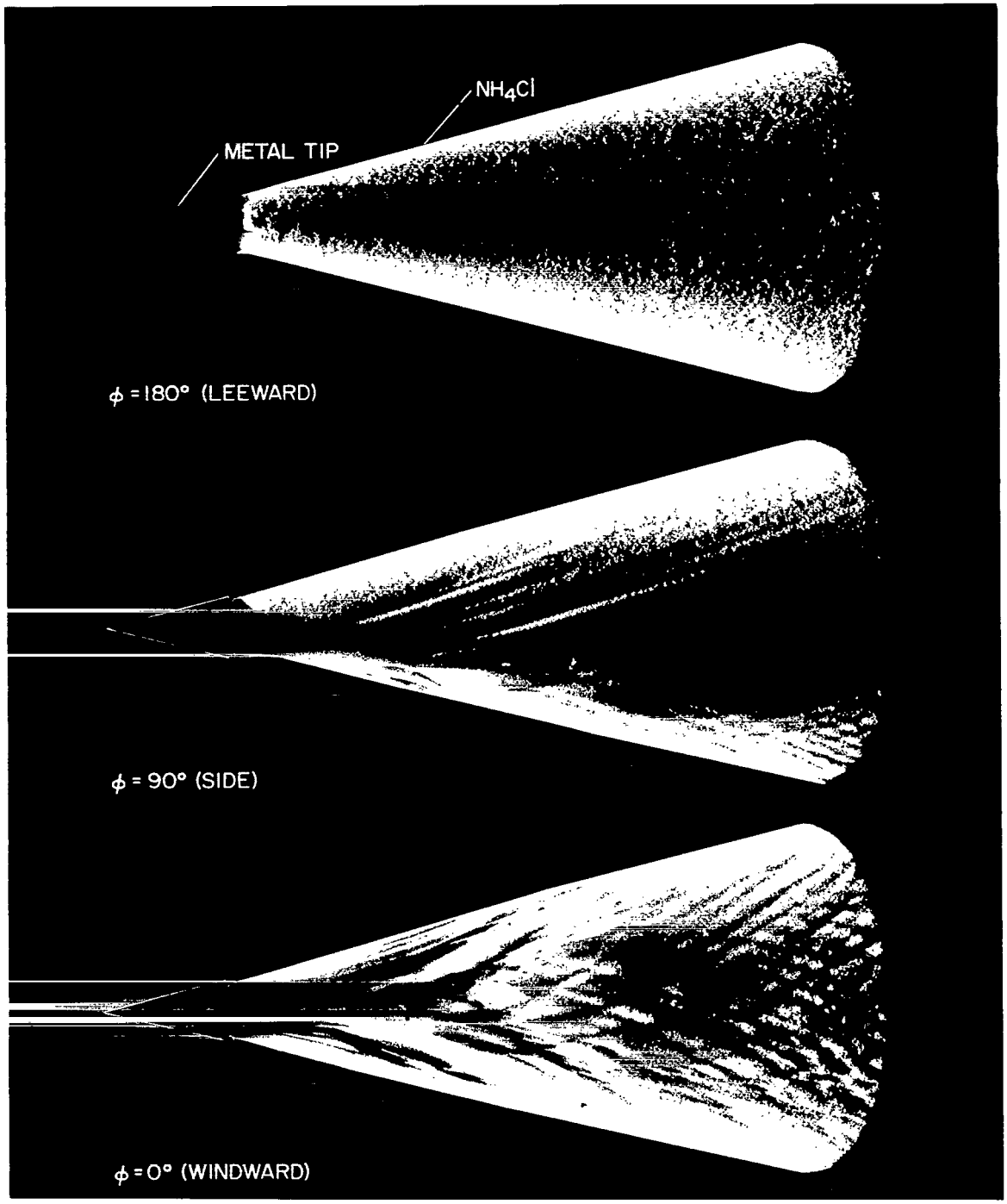

Figure 20.- Photographs of a 15° half-angle cone tested at an angle of attack of 10°; $M_\infty = 7.4$, $Re_{\infty,\ell} = 3\times10^6$, $\dot{m}/\rho_\infty U_\infty A_b \approx 0.001$.

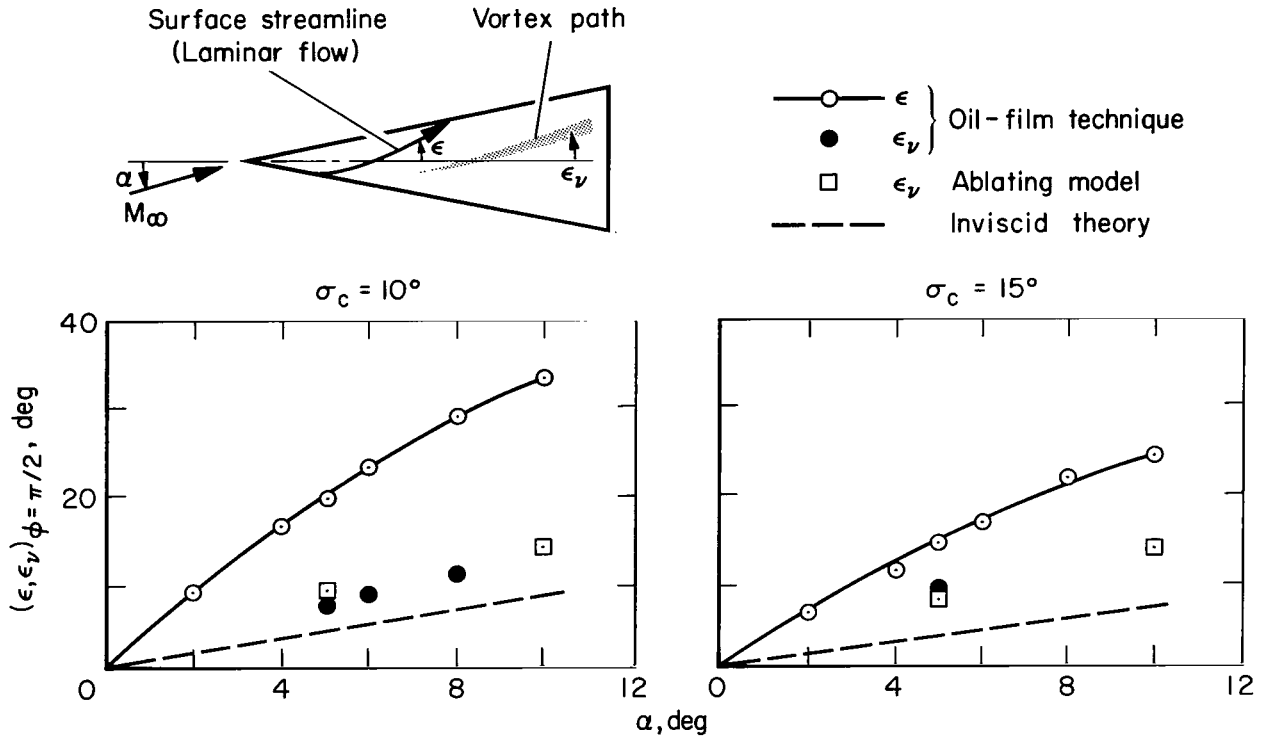

Figure 21.- Inclination of upwash grooves at cone side meridians and comparison with results from oil-film studies; M_∞ = 7.4 (air), $Re_{\infty,l} = 3\times10^6$.

NATIONAL AERONAUTICS AND SPACE ADMINISTRATION
WASHINGTON, D.C. 20546

OFFICIAL BUSINESS

FIRST CLASS MAIL

POSTAGE AND FEES PAID
NATIONAL AERONAUTICS AND
SPACE ADMINISTRATION

[illegible]

[illegible]

POSTMASTER: If Undeliverable (Section 158 Postal Manual) Do Not Return

"The aeronautical and space activities of the United States shall be conducted so as to contribute . . . to the expansion of human knowledge of phenomena in the atmosphere and space. The Administration shall provide for the widest practicable and appropriate dissemination of information concerning its activities and the results thereof."

—NATIONAL AERONAUTICS AND SPACE ACT OF 1958

NASA SCIENTIFIC AND TECHNICAL PUBLICATIONS

TECHNICAL REPORTS: Scientific and technical information considered important, complete, and a lasting contribution to existing knowledge.

TECHNICAL NOTES: Information less broad in scope but nevertheless of importance as a contribution to existing knowledge.

TECHNICAL MEMORANDUMS: Information receiving limited distribution because of preliminary data, security classification, or other reasons.

CONTRACTOR REPORTS: Scientific and technical information generated under a NASA contract or grant and considered an important contribution to existing knowledge.

TECHNICAL TRANSLATIONS: Information published in a foreign language considered to merit NASA distribution in English.

SPECIAL PUBLICATIONS: Information derived from or of value to NASA activities. Publications include conference proceedings, monographs, data compilations, handbooks, sourcebooks, and special bibliographies.

TECHNOLOGY UTILIZATION PUBLICATIONS: Information on technology used by NASA that may be of particular interest in commercial and other non-aerospace applications. Publications include Tech Briefs, Technology Utilization Reports and Notes, and Technology Surveys.

Details on the availability of these publications may be obtained from:

SCIENTIFIC AND TECHNICAL INFORMATION DIVISION

NATIONAL AERONAUTICS AND SPACE ADMINISTRATION

Washington, D.C. 20546